

GA-A22861

**EVOLUTION OF 2D DEUTERIUM AND IMPURITY RADIATION
PROFILES DURING TRANSITIONS FROM ATTACHED TO
DETACHED DIVERTOR OPERATION IN DIII-D**

by

**M.E. FENSTERMACHER, S.L. ALLEN, D.N. HILL, R.C. ISLER,
C.J. LASNIER, A.W. LEONARD, T.W. PETRIE, G.D. PORTER,
W.P. WEST, D.G. WHYTE, and R.D. WOOD**

AUGUST 1998

DISCLAIMER

This report was prepared as an account of work sponsored by an agency of the United States Government. Neither the United States Government nor any agency thereof, nor any of their employees, makes any warranty, express or implied, or assumes any legal liability or responsibility for the accuracy, completeness, or usefulness of any information, apparatus, product, or process disclosed, or represents that its use would not infringe privately owned rights. Reference herein to any specific commercial product, process, or service by trade name, trademark, manufacturer, or otherwise, does not necessarily constitute or imply its endorsement, recommendation, or favoring by the United States Government or any agency thereof. The views and opinions of authors expressed herein do not necessarily state or reflect those of the United States Government or any agency thereof.

**EVOLUTION OF 2D DEUTERIUM AND IMPURITY RADIATION
PROFILES DURING TRANSITIONS FROM ATTACHED TO
DETACHED DIVERTOR OPERATION IN DIII-D**

by

**M.E. FENSTERMACHER,[†] S.L. ALLEN,[†] D.N. HILL,[†] R.C. ISLER,[‡]
C.J. LASNIER,[†] A.W. LEONARD, T.W. PETRIE, G.D. PORTER,[†]
W.P. WEST, D.G. WHYTE,[◇] and R.D. WOOD[†]**

This is a preprint of a paper to be presented at the 13th International Conference on Plasma Surface Interactions on Controlled Fusion Devices, May 18–23, 1998, San Diego, California and to be published in *Journal of Nuclear Materials*.

[†]Lawrence Livermore National Laboratory

[‡]Oak Ridge National Laboratory

[◇]University of California, San Diego

**Work supported by
the U.S. Department of Energy
under Contracts DE-AC03-89ER51114, DE-AC05-96OR22464,
W-7405-ENG-48, and Grant DE-FG03-95ER54294**

**GA PROJECT 3466
AUGUST 1998**

ABSTRACT

This paper presents the detailed evolution of conditions along both the inner and outer divertor legs during the transition from attached ELMing H-mode to partially detached divertor (PDD) operation in DIII-D. Visible emission profiles in a poloidal plane show that in ELMing H-mode prior to deuterium gas injection, CIII emission peaks in the inner SOL near the X-point and deuterium emission (from ionization and recombination) peaks at the inner target plate near the inner strike point (ISP). The spatial profiles of the recombination and ionization zones, determined by forming images of the ratio of intensities from simultaneous images of D_α and D_γ emission, show that recombination dominates the inner leg emission near the target; ionization dominates in a poloidally narrow zone upstream in the inner leg. After deuterium injection, when the PDD transition begins, the profiles of carbon visible emission show first an increase in the inner SOL near the X-point, followed by increases in emission in the lower regions of the outer leg. Deuterium emission at the transition onset decreases at the ISP and increases across the private flux region below the X-point. As the transition to PDD conditions proceeds the deuterium emission increases in the private flux region; recombination dominates near the floor and ionization higher near the X-point. Carbon emission appears along both divertor legs and at the X-point. In the final quasi-steady PDD state, the recombination emission in the outer leg is near the separatrix and along the target plate; emission from collisional excitation dominates in the upper part of the outer leg just below the X-point, and carbon emission is localized at the X-point. These results suggest that transport of neutral deuterium between the inner and outer divertor legs through the private flux region plays an important role in the initiation of outer leg detachment in DIII-D.

1. INTRODUCTION

Studies of the partially detached divertor (PDD) operating mode, induced by deuterium injection in DIII-D, have shown it to be a robust technique for reducing the peak heat and particle fluxes to the target plates [1]. This is one of the candidate solutions to the problem of excessive peak heat flux in future tokamak devices. Detailed characterization of the plasma conditions in this mode have been done [2] in an attempt to understand the physics processes which allow it to be sustained in a quasi-steady (ELMing) state. This paper examines the evolution of the divertor plasma from the attached ELMing H-mode prior to gas injection, through various intermediate conditions until the final quasi-steady conditions with a partially detached outer leg are established. Understanding this transition is important for determining the applicability of this solution to higher power density applications and future divertor geometries.

A physics model of the quasi-steady PDD conditions asserts that radiation near the X-point cools the outer leg sufficiently to produce: 1) significant charge exchange momentum losses from the plasma flowing in the outer leg, and 2) volume recombination of the ion flux before it reaches the target plate. The electron temperature throughout the outer divertor leg is low ($\sim 1\text{--}3$ eV) and the density is high ($\sim 2\text{--}4 \times 10^{20}$ m³) especially in the SOL radially outward from the separatrix. The radiation profile peaks near the X-point and spectroscopic analysis indicates that the majority (>80%) of the X-point radiation is due to carbon. Radiation farther down the outer leg towards the outer strikepoint (OSP) is due to deuterium (>50%). Simulations of this condition [3] done with the UEDGE code [4] indicate that the temperature is sufficiently low in the outer leg below the X-point that charge exchange and other ion-neutral processes can remove momentum from the plasma flowing towards the target plates. In these simulations, the flow velocity decreases sufficiently to make the transit time through the lower outer leg comparable to the deuterium recombination time in the high density, low temperature plasma. UEDGE shows that a large fraction of the deuterium ion flux in the outer leg recombines before reaching the target plates. This is consistent with the measurements of low target plate ion flux during the PDD phase.

The purpose of this paper is to examine the physics which initiates the transition to this PDD state. The paper will focus on 2D measurements of the evolution of emission from carbon and deuterium throughout the divertor from the ELMing H-mode through various intermediate profiles to the quasi-steady distributions in the PDD phase. The paper is organized as follows. Section 2 describes the diagnostics used to obtain emission data in the divertor and the analysis methods required to determine the relative contributions of recombination and excitation

radiation to the total deuterium emission. Section 3 presents results of the recombination analysis and details of the evolution of the profiles. The results are discussed and future plans are presented in Section 4.

2. DIAGNOSTIC MEASUREMENTS AND DATA ANALYSIS METHODS

The tangential TV system (TTV) on DIII-D [5] is now capable of acquiring image data from two emission lines simultaneously allowing comparisons of carbon versus deuterium profiles and generation of 2D profiles of deuterium recombination and excitation emission. This is the primary diagnostic for this study although data from other DIII-D diagnostics are used in the analysis, for example T_e and n_e in the divertor measured by a divertor Thomson scattering (DTS) system, reconstructions of 2D profiles of total radiated power measured by a 48-channel bolometer array with crossed views, VUV line emission measurements with a SPRED spectrograph viewing the divertor, and radial profiles of heat and particle flux on the target plates measured by infrared cameras (IRTV) and floor mounted Langmuir probes respectively. The TTV diagnostic produces an image of the DIII-D divertor with the center of the line of sight nearly tangent to the X-point. The acquisition rate is 60 fields/s (16.7 ms per image). A 2D profile of the emission is reconstructed from the 3D raw data using a least squares minimization technique [5]. Emission from various visible lines of deuterium, carbon and other impurities can be selected by placing interference filters in front of the camera. A beamsplitter is placed in the optics path to transfer the emission from the tokamak through two filters simultaneously and into two cameras. This produces simultaneous profiles of carbon (or other impurities) and deuterium for comparisons. The system is also used to measure emission from two deuterium visible lines (D_α , and either D_β or D_γ) simultaneously to look for indications of deuterium volume recombination as described below.

Emission from a plasma dominated by deuterium recombination can be distinguished from emission due to collisional excitation in an ionizing plasma by the ratio of intensities of multiple lines [6]. Recombination preferentially populates higher Δn transitions (shorter wavelength lines) compared with collisional excitation from the ground state. Here n is the principal quantum number. Therefore ratios of low Δn (e.g. Balmer D_α) to high Δn (e.g. Balmer D_β or D_γ) emission will be lower in a recombining plasma. For the conditions in the DIII-D divertor, $T_e \sim 1-3$ eV, $n_e \sim 2-4 \times 10^{20} \text{ m}^{-3}$, the ratio of the D_α to D_γ lines is more than a factor of 20 lower in a recombining plasma compared with an ionizing plasma. The reconstructed 2D profile data from multiple images of the TTV system are used to generate an image of the D_α/D_γ ratio. The fraction of the emission due to recombination, F_r , is calculated at each image pixel from $F_r = R/(1 + R)$. Here R is the ratio of the observed photons due to recombination normalized to the photons from excitation as given by [6],

$$R = S_r/S_i = (\rho_m/\rho_i - 1)/(1 - \rho_m/\rho_r) \quad (1)$$

where ρ_m is the measured intensity ratio, ρ_i and ρ_r are the limiting ratios for purely ionizing and recombining plasmas, respectively. The fraction due to ionization is $F_i = 1 - F_r$. The limiting ratios ρ_i and ρ_r depend on both electron temperature (strong variation at low $T_e \sim 1-2$ eV) and density (weak dependence for $n_e > 1 \times 10^{20} \text{ m}^{-3}$). 2D profiles of T_e and n_e from divertor Thomson scattering, reconstructed from data obtained in discharges with radial sweeping of the divertor, are used to evaluate ρ_i and ρ_r at the location corresponding to each pixel in the reconstructed TTV image. Images of the emission in a poloidal plane (e.g. D_α) due to recombination versus that due to ionization are made by multiplying the fraction associated with each process at each pixel times the total emission.

3. EVOLUTION OF 2D CARBON AND RECOMBINATION/IONIZATION PROFILES

The temporal history of a typical high power DIII-D discharge with a PDD phase induced by a constant deuterium gas injection level (Fig. 1) shows that after the start of gas injection ($t_{\text{gas}} = 1900$ ms) the transition to PDD operation begins approximately 200 ms later (2100 ms); quasi-steady conditions of the peak heat flux are observed from 700 ms after the transition begins (2800 ms) to the end of the discharge. After the current flattop is reached (1100 ms), 14 MW of neutral beam power are injected to establish an ELMing H-mode plasma. The ELM frequency in this high power discharge is $f_{\text{ELM}} \sim 240$ Hz so images from the TTV integrate over several ELMs. Deuterium gas is injected into the SOL near the midplane at a rate of ~ 85 Tl/s. The outer target plate peak heat flux decreases 200 ms after t_{gas} indicating the transition to a partially detached outer leg. Bolometer reconstructions show that prior to the transition, local maxima of approximately equal radiation level exist along the inner leg from the ISP to the X-point and also at the OSP. The quasi-steady PDD operation with outer leg heat flux reduced by a factor of 4 (from ~ 400 MW/m² in the pre-injection H-mode to ~ 100 MW/m²) is established 900 ms after t_{gas} and continues until the end of the discharge. After the transition the bolometers show radiation increases a factor of 2 at the OSP and a factor of 5 from midway up the outer leg to the X-point. Radiation decreases a factor of 2 along the inner leg. The density rises about 10% during the quasi-steady phase; the confinement factor decreases during this time from $H_{89p} = 1.7$ to 1.45. Divertor Thomson scattering measurements show that T_e drops to < 2 eV at the transition up to $Z_x = 3$ cm above the target plate near the OSP. At $Z_x = 5$ cm T_e remains above 2 eV for 900 ms; at $Z_x = 7$ cm for 1400 ms and at $Z_x = 10$ cm for 2200 ms. This gradual cooling of the outer leg plasma is consistent with the deuterium emission profiles as described below.

Reconstructions of the 2D profiles of CIII (465 nm) emission (Fig. 2) show multiple phases from 1) emission primarily in the inner SOL near the X-point during ELMing H-mode [Fig. 2(a)] to 2) emission throughout the outer leg SOL during the transition to PDD operation, [Figs. 2(b) and 2(c)], and finally 3) localized emission near the X-point during the quasi-steady PDD phase [Fig. 2(d)]. Prior to gas injection [Fig. 2(a)] the emission from CIII is observed along the inner leg and near the X-point. Previous analysis of divertor SPRED data [7] and UEDGE code simulations [3] indicate that the temperature in the region of CIII emission is in the range 6–8 eV. The first frame of the TTV data to show a significant change in the profile occurs approximately 200 ms after t_{gas} [Fig. 2(b)]. The CIII emission increases both in the inner leg SOL and along the outer leg. During the transition the emission near the X-point increases [Fig. 2(c)] and there continues to be substantial emission along the outer leg and part way down

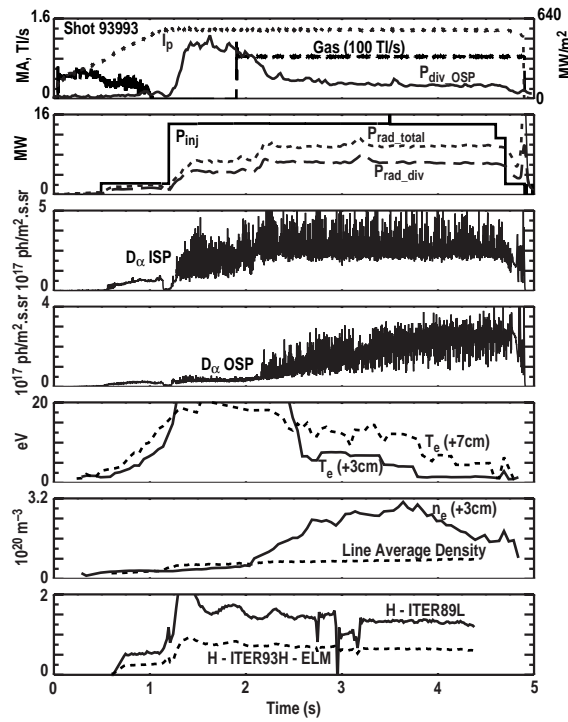


Fig. 1. Time history of DIII-D discharge 93993 showing (a) plasma current, I_p , gas injection, Gas, and outer leg peak heat flux, P_{div_OSP} , (b) injected neutral beam power, P_{inj} , total radiated power, P_{rad_total} and divertor radiated power, P_{rad_div} , (c) D_{α} emission from the inner strikepoint, D_{α_ISP} , (d) D_{α} emission from the outer strikepoint, D_{α_OSP} , (e) electron temperature at the DTS locations 3 cm and 7 cm above the vessel floor respectively, (f) divertor density 3 cm above the vessel floor and line averaged electron density, and (g) core energy confinement time normalized to ITER89P L-mode scaling and ITER93H ELMing H-mode scaling respectively.

the inner leg. The increase in CIII emission in the upper regions of the outer leg is consistent with DTS measurements showing T_e in this region in the 6–8 eV range during the transition. Finally, the profile during the quasi-steady PDD phase [Fig. 2(d)] shows emission primarily at the X-point and little emission along either divertor leg. Even though the peak appears somewhat inside the separatrix, this is a quasi-steady profile (with variations due to ELMs) for times long compared with an energy confinement time and core energy confinement is not significantly degraded (see Fig. 1).

Reconstructions and analysis of the D_{α} emission show that an ionization zone exists poloidally upstream of the recombination zone and that the locations of these zones are in the inner leg near the ISP during ELMing H-mode (pre-puff) and in the outer leg along the separatrix during PDD operation. The D_{α} emission due to recombination is shown in Fig. 3 and that due to collisional excitation in the ionizing regions of the plasma is shown in Fig. 4. Comparing the profiles during ELMing H-mode [recombination emission in Fig. 3(a) and ionization emission in Fig. 4(a)] shows that the recombination zone is close to the inner target

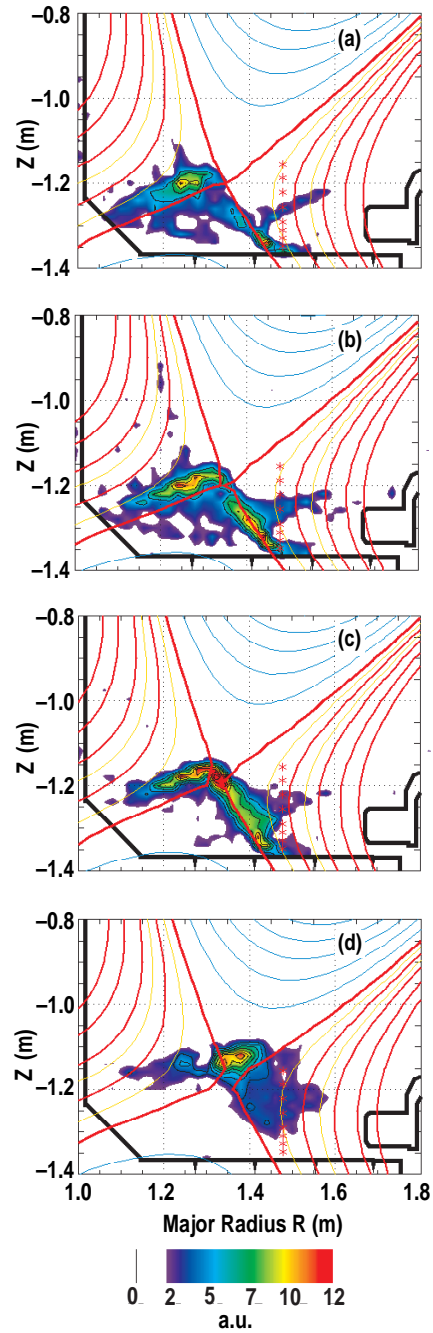


Fig. 2. Profiles of CIII emission (465 nm) from discharge 93992; (a) at 1889 ms during the ELMing H-mode phase, (b) at 2040 ms; the first frame to exhibit substantial change after the deuterium injection (at 1900 ms), (c) at 2107 ms during the transition to PDD conditions and (d) at 4085 ms during the quasi-steady PDD phase.

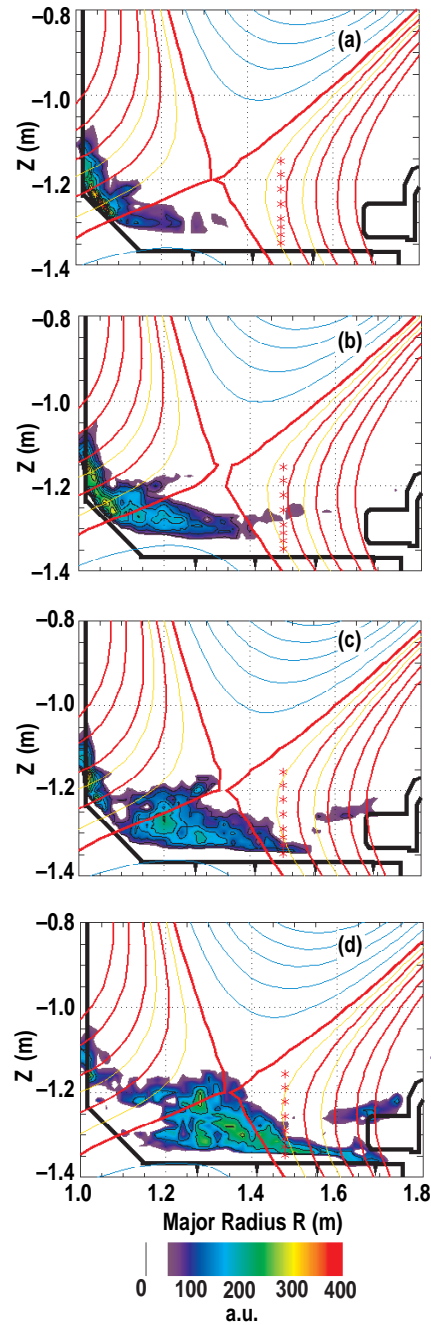


Fig. 3. Profiles of D_{α} emission (656.3 nm) due to recombination from discharge 93993; (a) at 1886 ms during the ELMing H-mode phase, (b) at 2088 ms; the first frame to exhibit substantial change after the deuterium injection (at 1900 ms), (c) at 2356 ms during the transition to PDD conditions and (d) at 3814 ms during the quasi-steady PDD phase.

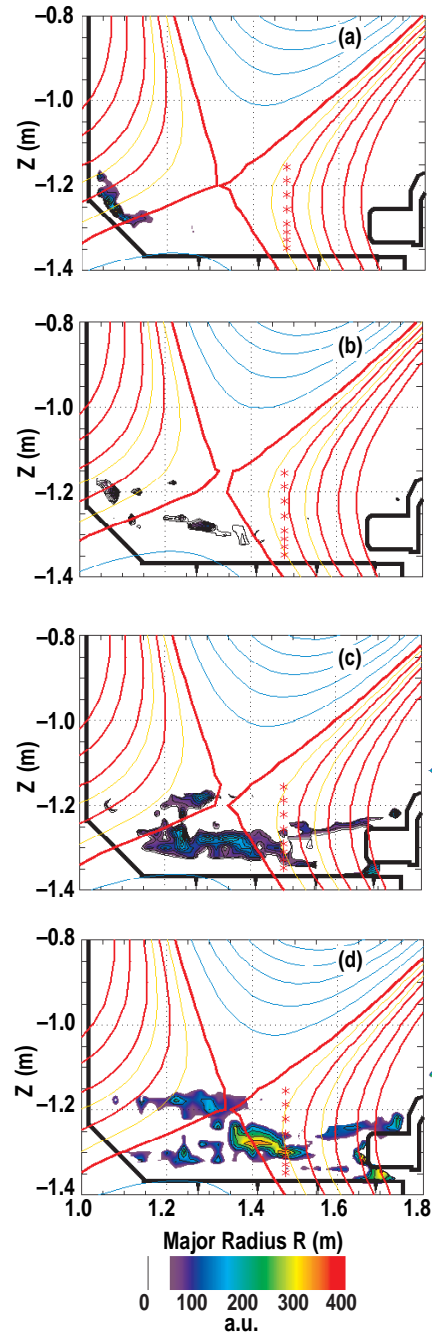


Fig. 4. Profiles of D_{α} emission (656.3 nm) due to collisional excitation in the ionizing plasma regions from discharge 93993; (a) at 1886 ms during the ELMing H-mode phase, (b) at 2088 ms; the first frame to exhibit substantial change after the deuterium injection (at 1900 ms), (c) at 2356 ms during the transition to PDD conditions and (d) at 3815 ms during the quasi-steady PDD phase.

plate and the ionization zone is several centimeters poloidally above the target plate in the inner leg. The shape of the ionization zone is consistent with UEDGE simulations [3] in which the contour of 5 eV electron temperature is closer to the target plate near the inner separatrix and farther from the target in the inner leg SOL (“flame front”). After gas injection, the first frames which show substantially different profiles are presented in Figs. 3(b) and 4(b). The emission due to recombination in particular shows an increase in the private flux region near the inner leg separatrix. Some increase in ionization emission in the PF region is also observed although the signal to noise ratio is poor. After 270 ms of transition, the profiles [Figs. 3(c) and 4(c)] show substantial emission throughout the private flux region. The emission due to recombination is larger nearer the floor of the PF region; the emission from ionization occurs vertically higher nearer the X–point. Finally, in the quasi-steady PDD phase [Figs. 3(d) and 4(d)], substantial emission due to recombination is observed in the outer divertor leg near the separatrix and in the PF region on the outer leg side. Emission from ionization occurs farther up the outer leg poloidally toward the X–point and is spread across the SOL. In this case the ionization emission is closest to the target plate on flux surfaces somewhat out into the SOL [approximately the 7.5 mm surface mapped to the midplane in Fig. 4(d)]. These images are consistent with Thomson scattering measurements showing low temperature ($T_e < 2$ eV) in the regions dominated by recombination and $T_e \sim 5$ eV higher off the target plate in the thin poloidal zone dominated by ionization. These measurements also imply that a deuterium ion flow should exist from the upper part of the outer leg (ionization source zone) to the lower region near the target (recombination sink) consistent with recent theories of convection dominated energy transport in the detached outer leg [9].

4. DISCUSSION AND FUTURE WORK

The evolution of the emission profiles of carbon and deuterium during the transition from ELMing H-mode to radiative divertor operation suggests that transport of neutral deuterium between the inner and outer divertor legs through the private flux region plays an important role in the initiation of detachment of the outer leg and subsequent heat flux reduction there. This spectroscopic evidence is consistent with previous observations using limited diagnostics [1,8]. During the ELMing H-mode phase, the emission from deuterium neutrals (both from ionization and recombination) appears in the inner leg near the ISP. This is consistent with the picture that the inner leg is nearly detached but still hot enough near the separatrix to ionize neutrals from the inner wall region and prevent them from filling the private flux region. Previous DTS data [10], in experiments with lower X-point height and radial sweeps of the divertor which produced DTS measurements of the inner leg in the pre-puff ELMing H-mode, showed $T_e \sim 5$ eV at the ISP; T_e lower farther out in the inner leg SOL and T_e higher along the separatrix toward the X-point. After gas puffing, the emission profiles indicate that neutrals enter the private flux region from the inner separatrix side, near the ISP at first, and during the transition the emission from neutrals fills the private flux region. DTS data from the PF region in discharges with radial sweeps show substantial electron density there ($n_e \sim 10^{20} \text{ m}^{-3}$) and very low $T_e < 1$ eV. Pressure measured in the PF region during the transition in these high injected power discharges is in the 20–30 mTorr range. The rapid bursts of power and particles into the divertor due to ELMs may play an important role in producing these conditions in the PF region. Finally, detachment of the outer leg corresponds to the time at which neutral emission begins to enter the outer leg across the separatrix from the PF side near the OSP. DTS measurements show that at this point the temperature near the OSP drops to the 1–3 eV range. The emission profiles of CIII show a decrease in the outer leg near the OSP and evolution of the emission to farther up the leg towards the X-point as the outer leg separatrix cools. As the transition continues to completion, the profiles of neutral emission show increases farther up the outer leg along the separatrix.

These observations lead to the conclusion that insertion of a baffle and/or pump in the private flux region of DIII-D could significantly change the parameters at which the outer leg detaches, the evolution of the transition to PDD operation, and possibly the effect of partially detached operation on core confinement. If neutral transport from the ISP to the OSP is completely blocked by baffling, heavy gas injection may trap neutrals between the inner separatrix and the baffle until the inner leg detaches completely up to the X-point. If the neutrals penetrate the core at this stage, before the outer leg detaches and heat flux is reduced, confinement may be

adversely affected. Conversely, if the baffle and pumping structure is designed to allow careful control of the transport of neutrals from ISP to OSP, the degree of partial detachment of the outer leg may be controllable in such a way that more nearly uniform radiation can be achieved. Careful consideration must also be given to the question of whether the control of the neutral flow through the baffled/pumped PF region requires variations in the separatrix to baffle gaps, since the interaction with the divertor leg plasmas of both neutrals and the carbon sputtered from the baffle will be affected by changes in the separatrix position. An independent control of the neutral flow at fixed configuration seems desirable.

This analysis is only the first step in extracting information from the time dependent profiles of carbon and deuterium emission. Existing data will be processed to examine the dependence of the profile evolution on the injected neutral beam power. This power scan will provide discharges with a range of ELM frequencies so that the effect of ELMs on the emission profiles, especially those from deuterium, can be examined. Cross calibration of the TTV data against absolutely calibrated line integrated measurements will also be done. When combined with n_e and T_e measurements from DTS this may allow profiles of the neutral density in the divertor to be generated for comparison with neutral transport simulations.

REFERENCES

- [1] T.W. Petrie, *et al.*, *Proc. 18th European Conf on Control Fusion and Plasma Phys.*, Berlin, Vol. **15c**, Part III (1991) 237; T.W. Petrie, *et al.*, *J. Nucl. Mater.* **196-198** (1992) 848; T.W. Petrie, *et al.*, *Nucl. Fusion* **37** (1997) 321.
- [2] M.E. Fenstermacher, *et al.*, *Phys. Plasmas* **4** (1997) 1761; M.E. Fenstermacher, *et al.*, *J. Nucl. Mater.* **241-243** (1997) 666.
- [3] G.D. Porter *et al.*, *Proc. 23rd European Conf on Control Fusion and Plasma Phys*, Kiev, Ukraine, p. 699, 1996, G.D. Porter, *et al.*, *Proc. 25th European Conf on Control Fusion and Plasma Phys*, Prague, Czech Republic, 1998 (in press).
- [4] T.D. Rognlien, *et al.*, *J. Nucl. Mater.* **196-198** 347 (1992).
- [5] M.E. Fenstermacher, *et al.*, *Rev. Sci. Instrum.* **68** (1997) 974.
- [6] R.C. Isler, *et al.*, *Phys. of Plasmas* **4** (1997) 2989.
- [7] R.D. Wood, *et al.*, *Proc. 23rd European Conference on Controlled Fusion and Plasma Physics*, Kiev, Ukraine, (1996) 763.
- [8] Ph. Ghendrih, *et al.*, *J. Nucl. Mater.* **220-222** (1995) 305, Ph. Ghendrih *et al.*, *Proc. 15th Int. Conf on Plasma Phys and Control. Nucl. Fus. Res.*, Seville, Vol. **3** (1994) p. 441.
- [9] A.W. Leonard, *et al.*, *Phys. Rev. Lett.* **78** 4769 (1997), A.W. Leonard, *et al.*, *Phys. Plasmas* **5** 1736 (1998).
- [10] S.L. Allen, *et al.*, *J. Nucl. Mater.* **241-243** (1997) 595.

ACKNOWLEDGMENT

Work supported by U.S. Department of Energy under Contract Nos. DE-AC03-89ER51114, W-7405-ENG-48, DE-AC05-96OR22464, and Grant No. DE-FG03-95ER54294.